RSC Medicinal Chemistry

ROYAL SOCIETY OF CHEMISTRY

RESEARCH ARTICLE

Cite this: DOI: 10.1039/d4md00670d

Antibacterial activity of the structurally novel C-2 amine-substituted analogues based on quinoxaline†

Yuting Liu,[ab] Pengju Yang,[ab] Yunyun Zhou[c] and Zhiwen Zhou *[ab]

In the current study, we have designed and prepared a series of quinoxaline-based compounds, which were derived from *o*-phenylenediamine. Among them, compounds **5m–5p** displayed good to moderate antibacterial activity with MICs of 4–16 μg mL^{-1} against *S. aureus*, 8–32 μg mL^{-1} against *B. subtilis*, 8–32 μg mL^{-1} against MRSA and 4–32 μg mL^{-1} against *E. coli*, respectively. Compound **5p**, identified as a potent broad-spectrum antibacterial agent, demonstrated the strongest inhibitory effects against a range of bacterial strains and low cytotoxicity, thereby warranting further investigation. Compound **5p** not only demonstrated the ability to disperse established bacterial biofilms but also induced a slower development of bacterial resistance compared to norfloxacin. Moreover, bactericidal time-kill kinetic studies revealed that at a high concentration of 3MIC, compound **5p** was capable of directly killing MRSA cells. The subsequent postcontact effect (PCE) results showed that the growth rate of viable bacteria (MRSA) was greatly impacted and did not recover in less than 24 hours, even after antibacterial agent **5p** was removed. The drug-like properties and ADME prediction exhibited that **5m–5p** obeyed Lipinski's rule of five and therefore presumably maintained moderate to good bioavailability and human intestinal absorption rate when administered orally. Mechanistic investigations have elucidated that compound **5p** exerted its antibacterial effect by compromising the structural integrity of bacterial cell membranes, resulting in the leakage of intracellular constituents and ultimately causing bacterial demise. Further studies *in vivo* have demonstrated that **5p** exhibited potent antibacterial efficacy against MRSA in murine corneal infection models, particularly at elevated concentrations. The current dataset has also been meticulously analyzed to delineate the structure–activity relationships (SARs) of the synthesized compounds.

Received 29th August 2024,
Accepted 31st October 2024

DOI: 10.1039/d4md00670d

rsc.li/medchem

Introduction

The increasing resistance of pathogens to current antibiotics highlights the need for ongoing research into novel antimicrobials. Antibiotic-resistant pathogenic bacterial infections kill an estimated 700 000 individuals worldwide each year.[1] Moreover, as a result of the extensive use and misuse of antibiotics, the treatment of drug-resistant bacteria has become a worldwide problem.[2] Thus, there is an urgent necessity for the creation of new antibacterial agents with unique structures and a mode of action that may differ from that of present first-line antimicrobial treatments.

Quinoline nuclei are chemically useful synthons bearing diverse biological activities, including antimicrobial,[3] analgesic,[4] anticancer[5] and anti-inflammatory activity.[6] Recently, some quinoline-derived compounds have been designed and synthesized to investigate the SARs of the hybrid compounds (Fig. 1).[7–11] The results showed that most of the derivatives are potent antibacterial agents against several strains of Gram-positive bacteria, including multidrug-resistant (MDR) clinical isolates (Fig. 1). Structure–activity relationship (SAR) studies of these derivatives have indicated that introducing a primary or secondary amino group greatly influences their antibacterial potency, spectrum and safety. It is generally believed that the action of quinoline-derived compounds increases with an increase in hydrophilicity.[12] This is most likely due to the amino residue producing a cation configuration, which gives a considerable advantage in avoiding bacterial resistance.[13,14] As a result, introducing one or more amino groups into the parent nucleus of quinoline might considerably improve the water solubility of the compounds and so boost their antibacterial activity, which will provide us with a new idea for the next

[a] *Third-grade Pharmacological Laboratory on Traditional Chinese Medicine, State Administration of Traditional Chinese Medicine, China Three Gorges University, Yichang, 443002, China. E-mail: zhiwen.zhou@hotmail.com; Tel: +86 717 6397328*
[b] *Department of Pharmacy, College of Medicine and Health Sciences, China Three Gorges University, Yichang, 443002, China*
[c] *Department of Quality Control, China Resources Sanjiu (Huangshi) Medical & Pharmaceutical Co., Ltd., Huangshi, China*

† Electronic supplementary information (ESI) available. See DOI: https://doi.org/10.1039/d4md00670d

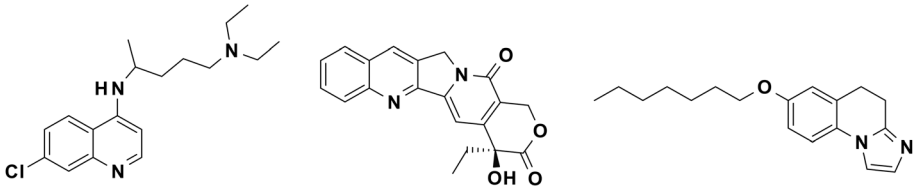

Fig. 1 Some quinoline-derived compounds displaying good antimicrobial activity.

modification. Furthermore, some of the derivatives exhibit excellent *in vivo* antibacterial activity against *S. aureus* with competitive binding to chloramphenicol, suggesting that its anchor group reaches chloramphenicol-binding sites in the peptidyl transferase center (PTC).[15] These investigations demonstrated that quinoline-based derivatives have the potential to be promising antibacterial leads and require further research.

The emergence of bacterial resistance has significantly undermined the therapeutic potential of quinoline-based derivatives, including quinolone antimicrobial agents. Bacterial resistance to quinolones mainly involves the colonization, biofilm formation and spread of antibiotic-resistant genes in the pathogenic strains.[16] In addition, the efflux pump encoded by the *mef* gene pumps quinolones out of intracellular space and prevents them from reaching the binding sites.[17] Consequently, this issue of bacterial resistance drives further research in designing novel quinoline-based antibacterial agents. Furthermore, these quinoline-based derivatives also displayed certain drawbacks, including reduced bioavailability, probably due to their low water solubility, and limited antibacterial spectrum mainly against Gram-positive bacteria.

The incorporation of bioisostere into molecules is a typical approach of modifying structures, and numerous drugs such as antibacterial fluoroquinolones, fluorouracil, and procainamide have employed this design principle in their development.[18,19] Therefore, in the current work, we also applied the principle of bioisosterism to substitute C-4 in the quinoline ring with a nitrogen atom, obtaining the parent nucleus of quinoxaline (Fig. 2). The introduction of a nitrogen atom or amino group can obviously improve the water solubility, antibacterial potency and spectrum and safety of quinoxaline. Inspired by these research results, we opted to structurally modify quinoxaline at C-2 and C-3 by inserting amino groups at both positions in order to produce derivatives with stronger antibacterial activity, improved water solubility, and a broader antibacterial spectrum (Fig. 2). This study also investigated the mechanism of antibacterial activity in its preliminary stage.

Experimental

General

The majority of the chemical reagents and solvents utilized in the experiments were of analytical grade and underwent purification according to standardized protocols. The melting points were determined using a micro-melting point apparatus, model XT-4, manufactured in Shanghai, China. Proton (^{1}H NMR) and carbon (^{13}C NMR) nuclear magnetic resonance spectra were acquired on a Bruker AV-300 spectrometer located in Berlin, Germany, with trimethylsilane (TMS) serving as the internal reference standard. The chemical shift values were reported in parts per million (ppm) relative to TMS, and the coupling constants were expressed in hertz (Hz). High-resolution mass spectrometry data were generated using an Agilent QTOF 6520 mass spectrometer from New York, USA. Fluorescence measurements were conducted with an F-7000 spectrofluorimeter provided by Hitachi, Tokyo, Japan. Ultraviolet (UV) absorption spectra were recorded at ambient temperature using a TU-2450 spectrophotometer from Puxi Analytic Instrument Co., Ltd., Beijing, China.

General procedure for the synthesis of 5a–5p. Compound **1** (864 mg, 8 mmol) was dissolved in a 3.5 M hydrochloric acid solution (20 mL). To this solution, glycolic acid (864 mg, 9.6 mmol) was introduced and the resulting mixture was subjected to reflux for about 8 hours. After that, the reaction mixture was allowed to cool to ambient temperature. Subsequently, an aqueous ammonia solution was incrementally added to the mixture until the pH reached a neutral value of 7.3. The precipitate formed was then isolated by filtration. The crude product was further purified through recrystallization using a 70% ethanol–water solvent system, yielding a yellow powder, designated as compound **2** (972 mg, 5.9 mmol), with an overall yield of 75%.

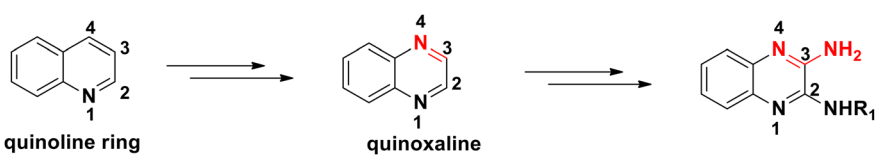

Fig. 2 Design concept of the quinoxaline derivatives.

Compound **2** (972 mg, 5.9 mmol) was dissolved in 1,2-dichloroethane (28 mL), to which dichlorosulfoxide (3 mL) and a catalytic amount of DMF were added. The reaction mixture was heated under reflux for 6 hours and then subjected to vacuum drying to remove solvents. Following this, the reaction solution was diluted with ethyl acetate (100 mL) and the organic layer was sequentially washed with water and brine to remove inorganic impurities. The organic phase was subsequently dried over anhydrous sodium sulfate to remove residual water, filtered, and the solvent was evaporated under reduced pressure. The crude product was further purified by silica gel column chromatography using a dichloromethane–methanol solvent system with a ratio of 40 : 1. The purified product, designated as **3**, was obtained as a yellow solid (855 mg, 4.3 mmol), corresponding to a yield of 72%.

A solution of 2,3-dichloroquinoxaline **3** (855 mg, 4.3 mmol) was prepared in a mixture of ammonia in DMF (150 mL). This mixture was stirred at a controlled temperature of 0 °C for a period of 1.5 hours to facilitate the reaction. After that, the reaction mixture was filtered to remove any insoluble materials. The filtrate was then subjected to vacuum concentration to remove the solvents. The resulting residue was subsequently subjected to purification using silica gel column chromatography, employing a gradient elution with a dichloromethane–methanol solvent system in a ratio of 20 : 1. The purified product, identified as compound **4**, was obtained as a solid (664 mg, 3.7 mmol), with an overall yield of 85%.

Compound **4** (80 mg, 0.45 mmol) was dissolved in anhydrous ethanol (16 mL), to which diisopropylethylamine (DIEA) (0.20 mL, 0.9 mmol) and a primary amine (0.9 mmol, 2.0 eq.) were added. The resulting mixture was reacted under a temperature of r.t.–70 °C for a duration of 8 hours. After that, the mixture was dried under vacuum and then diluted with dichloromethane (100 mL). The organic layer was sequentially washed with water and brine, followed by drying over anhydrous sodium sulfate to remove residual moisture. The mixture was then filtered, and the filtrate was concentrated under reduced pressure. The crude product was subjected to purification *via* silica gel column chromatography, employing a gradient elution with a dichloromethane–methanol solvent system, varying from 20 : 1 to 50 : 1. The purified fractions were combined to yield the target compounds **5a**–**5p**.

*3-Amino-2-(1-cyclohexene ethylamine)-quinoxaline (**5a**).* White solid (59 mg, 48%). Mp. 138–142 °C; ^{1}H NMR (600 MHz, $CDCl_3$) δ 7.79 (d, J = 8.1 Hz, 1H), 7.75 (d, J = 8.1 Hz, 1H), 7.59 (t, J = 7.4 Hz, 1H), 7.39 (t, J = 7.5, 1H), 5.63 (s, 2H), 3.65 (q, J = 5.9 Hz, 2H), 2.40 (t, J = 6.4 Hz, 2H), 2.03 (d, 4H), 1.68–1.65 (m, 2H), 1.62–1.59 (m, 2H); ^{13}C NMR (151 MHz, $CDCl_3$) δ 148.0, 141.4, 137.9, 136.2, 134.7, 129.9, 128.0, 126.0, 124.9, 124.3, 38.9, 37.3, 27.8, 25.2, 23.0, 22.2; HR-MS (ESI) m/z: calculated for $C_{16}H_{21}N_4$ $[M + H]^+$: 269.1766, found: 269.1768.

*3-Amino-2-cyclohexyl ethylamine quinoxaline (**5b**).* White solid (62 mg, 51%). Mp. 148–151 °C; ^{1}H NMR (600 MHz, $CDCl_3$) δ 7.82 (d, J = 8.1 Hz, 1H), 7.76 (d, J = 8.1 Hz, 1H), 7.59 (t, J = 8.1 Hz, 1H), 7.39 (t, J = 8.1 Hz, 1H), 5.49 (s, 1H), 3.63 (q, J = 5.6 Hz, 2H), 1.75 (d, J = 2.0 Hz, 2H), 1.83–1.61 (m, 10H); ^{13}C NMR (151 MHz, $CDCl_3$) δ 147.9, 141.6, 138.0, 136.2, 130.0, 128.0, 125.8, 124.6, 39.3, 35.7, 33.4, 32.0, 29.8, 26.4, 26.4, 22.4; HR-MS (ESI) m/z: calculated for $C_{16}H_{23}N_4$ $[M + H]^+$: 271.1923, found: 271.1928.

*3-Amino-2-methylamino quinoxaline (**5c**).* White solid (44 mg, 56%). Mp. 128–130 °C; ^{1}H NMR (600 MHz, $CDCl_3$) δ 7.82 (d, J = 7.6 Hz, 1H), 7.76 (d, J = 7.5 Hz, 1H), 7.63 (q, J = 7.6 Hz, 2H), 3.03 (s, 3H); ^{13}C NMR (151 MHz, $CDCl_3$) δ 142.6, 139.5, 136.2, 135.8, 131.6, 129.8, 127.4, 126.3, 27.4.

*3-Amino-2-ethylamino quinoxaline (**5d**).* White solid (51 mg, 60%). Mp. 136–140 °C; ^{1}H NMR (600 MHz, $CDCl_3$) δ 7.69 (d, J = 8.0 Hz, 1H), 7.62 (d, J = 8.0 Hz, 1H), 7.58 (t, J = 7.8 Hz, 1H), 7.50 (t, J = 7.8 Hz, 1H), 3.01 (q, J = 5.1 Hz, 2H), 1.14 (t, J = 5.1 Hz, 3H); ^{13}C NMR (151 MHz, $CDCl_3$) δ 147.8, 141.3, 137.8, 137.3, 136.5, 132.4, 130.1, 128.8, 42.6, 34.5.

*3-Amino-2-phenethylamine quinoxaline (**5e**).* Yellow powder (49 mg, 42%). Mp. 155–157 °C; ^{1}H NMR (600 MHz, $CDCl_3$) δ 7.80 (d, J = 8.4 Hz, 1H), 7.73 (d, J = 8.4 Hz, 1H), 7.59 (t, J = 7.8 Hz, 1H), 7.39 (t, J = 7.8, 2H), 7.30 (d, J = 8.1 Hz, 2H), 7.24–7.19 (m, 2H), 5.66 (s, 1H), 3.91 (q, J = 5.9 Hz, 2H), 3.20 (t, J = 6.4 Hz, 2H); ^{13}C NMR (151 MHz, $CDCl_3$) δ 148.0, 141.2, 138.0, 136.4, 136.2, 134.1, 130.9, 129.9, 129.5, 128.3, 128.0, 126.9, 126.2, 124.9, 41.2, 32.7; HR-MS (ESI) m/z: calculated for $C_{16}H_{17}N_4$ $[M + H]^+$: 265.1453, found: 265.1460.

*3-Amino-2-phenylpropylamine quinoxaline (**5f**).* Yellow solid (59 mg, 45%). Mp. 173–176 °C; ^{1}H NMR (600 MHz, $CDCl_3$) δ 7.79 (d, J = 7.8 Hz, 1H), 7.75 (d, J = 7.8 Hz, 1H), 7.60 (t, J = 7.6 Hz, 1H), 7.45 (t, J = 7.6 Hz, 2H), 7.29 (d, J = 8.1 Hz, 2H), 7.21 (d, J = 8.1 Hz, 2H), 5.60 (s, 1H), 3.88 (q, J = 6.8 Hz, 2H), 3.02 (t, J = 6.8 Hz, 2H), 2.20–2.09 (m, 2H); ^{13}C NMR (151 MHz, $CDCl_3$) δ 148.0, 141.5, 138.0, 137.2, 136.3, 132.6, 130.3, 129.9, 129.0, 128.0, 125.9, 125.2, 41.2, 35.3, 30.6; HR-MS (ESI) m/z: calculated for $C_{17}H_{19}N_4$ $[M + H]^+$: 279.1610, found: 279.1612.

*3-Amino-2-(2-naphthalene methylamine)-quinoxaline (**5g**).* Yellow solid (55 mg, 41%). Mp. 189–193 °C; ^{1}H NMR (600 MHz, $CDCl_3$) δ 8.12 (d, J = 8.7 Hz, 1H), 7.94 (d, J = 8.7 Hz, 1H), 7.89–7.83 (m, 3H), 7.70 (t, J = 7.3 Hz, 1H), 7.59 (d, J = 7.1 Hz, 1H), 7.58–7.54 (m, 2H), 7.51 (t, J = 7.3 Hz, 1H), 7.49 (t, J = 7.3 Hz, 1H), 5.79 (s, 1H), 5.25 (d, J = 4.9 Hz, 2H). ^{13}C NMR (151 MHz, $CDCl_3$) δ 147.9, 141.1, 138.0, 136.2, 134.0, 133.1, 131.8, 129.9, 129.1, 129.0, 128.1, 126.7, 126.5, 125.9, 125.9, 125.3, 125.1, 123.7, 43.7; HR-MS (ESI) m/z: calculated for $C_{19}H_{17}N_4$ $[M + H]^+$: 301.1453, found: 301.1449.

*3-Amino-2-(2-fluoro phenylethylamine)-quinoxaline (**5h**).* Yellow solid (61 mg, 48%). Mp. 201–205 °C; ^{1}H NMR (600 MHz, $CDCl_3$) δ 7.82 (d, J = 7.9 Hz, 1H), 7.75 (d, J = 7.9 Hz, 1H), 7.59 (t, J = 7.2 Hz, 1H), 7.42 (t, J = 7.2, 1H), 7.29–7.24 (m, 2H), 7.15–7.09 (m, 2H), 5.69 (s, 1H), 3.89 (q, J = 6.3 Hz, 2H), 3.12 (t, J = 6.3, 2H); ^{13}C NMR (151 MHz, $CDCl_3$) δ 161.9, 160.3, 148.0, 141.2, 138.1, 136.6, 131.2, 131.2, 129.9, 128.6, 128.2, 128.0, 125.9, 124.8, 124.5, 124.3, 115.6, 115.3, 41.5, 28.7; HR-MS (ESI) m/z: calculated for $C_{16}H_{16}FN_4$ $[M + H]^+$: 283.1359, found: 283.1358.

*3-Amino-2-(4-fluoro phenylethylamine)-quinoxaline (**5i**).* Yellow solid (54 mg, 43%). Mp. 202–205 °C; ^{1}H NMR (600 MHz, $CDCl_3$) δ 7.82 (d, J = 7.9 Hz, 1H), 7.75 (d, J = 7.9 Hz, 1H), 7.59 (t, J = 7.2 Hz, 1H), 7.45 (t, J = 7.2 Hz, 1H), 7.28–7.26 (m, 2H), 7.10 (t, J = 8.1 Hz, 2H), 5.59 (s, 1H), 3.85 (q, J = 5.8 Hz, 2H), 3.02 (t, J = 5.8 Hz, 2H); ^{13}C NMR (151 MHz, $CDCl_3$) δ 162.3, 161.0, 147.7, 140.9, 137.7, 136.2, 134.3, 134.3, 129.9, 129.7, 129.7, 128.0, 125.9, 124.8, 115.7, 115.3, 42.6, 34.2.

*3-Amino-2-(2-bromo phenylethylamine)-quinoxaline (**5j**).* Yellow solid (64 mg, 42%). Mp. 193–197 °C; ^{1}H NMR (600 MHz, $CDCl_3$) δ 7.80 (d, J = 8.5 Hz, 1H), 7.74 (d, J = 8.5 Hz, 1H), 7.59 (t, J = 7.8 Hz, 2H), 7.39 (t, J = 7.8 Hz, 1H), 7.29–7.28 (m, 2H), 7.13–7.09 (m, 1H), 5.66 (s, 1H), 3.89 (q, J = 5.2 Hz, 2H), 3.19 (t, J = 5.2 Hz, 2H); ^{13}C NMR (151 MHz, $CDCl_3$) δ 148.0, 141.2, 138.5, 138.0, 136.3, 132.9, 130.9, 129.8, 128.5, 128.1, 127.7, 126.2, 124.9, 124.5, 41.5, 35.3; HR-MS (ESI) m/z: calculated for $C_{16}H_{16}BrN_4$ $[M + H]^+$: 343.0558, found: 343.0556.

*3-Amino-2-(4-bromo phenylethylamine)-quinoxaline (**5k**).* Yellow solid (60 mg, 39%). Mp. 200–204 °C; ^{1}H NMR (600 MHz, $CDCl_3$) δ 7.82 (d, J = 7.9 Hz, 1H), 7.77 (d, J = 7.9 Hz, 1H), 7.61 (t, J = 7.2 Hz, 1H), 7.50 (d, J = 7.8, 2H), 7.43 (t, J = 7.5 Hz, 1H), 7.20 (d, J = 7.8 Hz, 2H), 5.61 (s, 1H), 3.87 (q, J = 6.5 Hz, 2H), 3.01 (t, J = 6.3 Hz, 2H). ^{13}C NMR (151 MHz, $CDCl_3$) δ 147.7, 141.2, 138.0, 137.7, 136.4, 132.0, 130.6, 130.4, 128.1, 125.9, 125.3, 120.3, 42.6, 34.7.

*3-Amino-2-(3,4-dichlorophenylethylamine)-quinoxaline (**5l**).* Yellow solid (52 mg, 35%). Mp. 214–216 °C; ^{1}H NMR (600 MHz, $CDCl_3$) δ 7.88 (d, J = 8.5 Hz, 1H), 7.68 (t, J = 7.5 Hz, 1H), 7.55 (d, J = 7.6, 2H), 7.46 (t, J = 7.4 Hz, 1H), 7.25 (d, J = 7.1 Hz, 2H), 5.63 (s, 1H), 3.90 (q, J = 5.9 Hz, 2H), 3.12 (t, J = 6.1 Hz, 2H). ^{13}C NMR (151 MHz, $CDCl_3$) δ 149.5, 148.8, 139.1, 138.2, 137.3, 133.5, 131.8, 133.2, 129.7, 126.6, 126.2, 121.5, 43.0, 35.1.

*3-Amino-2-(4-methyl phenylethylamine)-quinoxaline (**5m**).* White solid (56 mg, 45%). Mp. 186–188 °C; ^{1}H NMR (600 MHz, $CDCl_3$) δ 7.81 (d, J = 8.1 Hz, 1H), 7.75 (d, J = 8.1 Hz, 1H), 7.59 (t, J = 7.2 Hz, 1H), 7.42 (t, J = 7.2, 1H), 7.19 (s, 4H), 5.62 (s, 1H), 3.90 (q, J = 5.9 Hz, 2H), 3.01 (t, J = 5.5 Hz, 2H), 2.40 (s, 3H); ^{13}C NMR (151 MHz, $CDCl_3$) δ 148.0, 141.5, 138.1, 136.6, 135.9, 135.5, 129.9, 129.3, 128.8, 128.0, 125.8, 125.0, 42.7, 34.8, 21.1; HR-MS (ESI) m/z: calculated for $C_{17}H_{19}N_4$ $[M + H]^+$: 279.1610, found: 279.1615.

*3-Amino-2-(4-methoxy phenylethylamine)-quinoxaline (**5n**).* White solid (72 mg, 55%). Mp. 203–206 °C; ^{1}H NMR (600 MHz, $CDCl_3$) δ 7.80 (d, J = 7.8 Hz, 1H), 7.76 (d, J = 7.8 Hz, 1H), 7.62 (t, J = 6.9 Hz, 1H), 7.39 (t, J = 6.9, 1H), 7.21 (d, J = 7.9 Hz, 2H), 6.89 (d, J = 7.9 Hz, 2H), 5.61 (s, 1H), 3.84 (q, J = 5.8 Hz, 2H), 3.83 (s, 3H), 3.01 (t, J = 5.6 Hz, 2H); ^{13}C NMR (151 MHz, $CDCl_3$) δ 158.2, 148.0, 141.5, 138.0, 136.2, 131.1, 129.9, 129.5, 128.0, 125.9, 125.1, 114.2, 55.4, 43.0, 34.3; HR-MS (ESI) m/z: calculated for $C_{17}H_{19}N_4O$ $[M + H]^+$: 295.1559, found: 295.1560.

*3-Amino-2-(3-methoxy phenylethylamine)-quinoxaline (**5o**).* White solid (58 mg, 44%). Mp. 198–203 °C; ^{1}H NMR (600 MHz, $CDCl_3$) δ 7.81 (d, J = 7.8 Hz, 1H), 7.74 (d, J = 7.8 Hz, 1H), 7.59 (t, J = 6.8 Hz, 1H), 7.43 (t, J = 6.8 Hz, 1H), 7.27 (t, J = 6.8 Hz, 1H), 6.91 (d, J = 7.1 Hz, 1H), 6.81 (d, J = 6.8 Hz, 2H), 5.63 (s, 1H), 3.89 (q, J = 6.5 Hz, 2H), 3.83 (s, 3H), 3.03 (t, J = 6.2 Hz, 2H); ^{13}C NMR (151 MHz, $CDCl_3$) δ 159.8, 148.0, 141.4, 140.6, 138.0, 136.6, 129.9, 129.5, 128.0, 125.9, 124.8, 121.2, 114.7, 111.9, 55.3, 42.8, 35.3.

*3-Amino-2-(4-tert-butyl phenylethylamine)-quinoxaline (**5p**).* Yellow solid (50 mg, 35%). Mp. 234–237 °C; ^{1}H NMR (600 MHz, $CDCl_3$) δ 7.89 (d, J = 8.1 Hz, 1H), 7.81 (d, J = 8.1 Hz, 1H), 7.65 (t, J = 8.1 Hz, 1H), 7.46–7.41 (m, 5H), 5.89 (s, 1H), 4.81 (d, J = 4.5 Hz, 2H), 1.40 (s, 9H); ^{13}C NMR (151 MHz, $CDCl_3$) δ 150.5, 147.8, 141.3, 137.8, 136.6, 134.9, 129.9, 128.1, 127.7, 125.9, 125.7, 124.9, 45.4, 34.5, 32.0, 31.4, 29.8, 22.5, 14.2; HR-MS (ESI) m/z: calculated for $C_{20}H_{25}N_4$ $[M + H]^+$: 321.2079, found: 321.2077.

Antibacterial activity and cytotoxicity assays

The antibacterial efficacy and cytotoxicity of the synthesized compounds were evaluated using established methodologies as previously described.[20] The minimum inhibitory concentrations (MICs) for a range of drug-sensitive bacterial strains, namely *Staphylococcus aureus* RN4220, *Bacillus subtilis* 168, *Escherichia coli* DH5α, and *Pseudomonas aeruginosa* PAO1 as well as drug-resistant strains including methicillin-resistant *S. aureus* (MRSA) USA300, vancomycin-resistant *Enterococci* (VRE), and *Klebsiella pneumoniae*, were determined using a standardized twofold dilution technique in lysogeny broth (LB) medium. The cytotoxicity of the compounds was assessed on human breast adenocarcinoma cells (MCF-7), human embryonic kidney cells (HEK-293), and human proximal tubule epithelial cells (HK-2) using the MTT assay. The cell lines and biochemical reagents used throughout the experiments were sourced from the Shanghai Institute of Medicine, affiliated with the Chinese Academy of Sciences.

Propensity to induce bacterial resistance

Compound **5p**, identified as the most potent in our study, was subjected to an investigation of the rate of bacterial resistance development, following established protocols from the literature.[21] Standard strains of MRSA and *E. coli* were serially subcultured starting from the initial MIC. Upon subculturing MRSA and *E. coli* in fresh medium, the MIC values were reassessed every 24 hours. Concurrently, positive control groups were exposed to twofold dilutions of reference antibiotics as per standard procedures. This experimental regimen was maintained for a period of 24 days.

Bactericidal time-kill kinetics

The MRSA and *E. coli* cells were incubated at 37 °C for 24 hours and 36 hours, respectively, followed by adjustment to a concentration of approximately 2×10^6 CFU mL^{-1}. Bacterial suspensions (1 mL) were then treated with compound **5p** at varying concentrations: for MRSA, at 2× MIC and 3× MIC; for *E. coli*, at 3× MIC. After treatment, the suspensions were

further cultured at 37 °C with continuous shaking. At specific time points (0.5, 1, 2, 3, 5, 7, 9, 11, and 13 hours), 100 μL aliquots were removed from the cultures, serially diluted 10 times in phosphate-buffered saline (PBS), and spread onto sterile Mueller–Hinton agar plates. These plates were incubated for an additional 24 hours at 37 °C to allow for bacterial colony formation. The resulting bacterial colony counts were recorded after incubation. To ensure reliability, the experiments were conducted in duplicate.

Biofilm disruption assay

MRSA and *E. coli* cultures in the mid-logarithmic phase were suspended to a concentration of 2×10^6 CFU mL^{-1}. Aliquots of the suspension (100 μL) were then plated and incubated under standardized conditions for 48 hours for MRSA and *E. coli*. Following incubation, the spent culture medium was aspirated, and the bacterial cells were gently washed with phosphate-buffered saline (PBS) to remove any loose cells. Subsequently, compound **5p** (100 μL) at varying concentrations (for MRSA: MIC, 2× MIC and 3× MIC; for *E. coli*: MIC, 2× MIC and 4× MIC) was added to the wells containing the established biofilms, and incubation was continued for an additional 24 hours. A control group, in which 100 μL of sterile medium replaced compound **5p**, was also included. After the treatment, the culture solution was removed, and the unadhered cells were washed off with PBS. To disperse the biofilms, 100 μL of a trypsin–EDTA mixture was added to the treated bacterial cells. The ability of the biofilm to disperse was evaluated by performing serial 10-fold dilutions of the cell suspension on agar plates. Following a 24-hour incubation period, the number of colonies was meticulously counted, and the total bacterial count was expressed as $\log_{10}$ CFU mL^{-1}. The results were then compared with those of the control group to assess the efficacy of compound **5p** against biofilm formation.

Evaluation of postcontact effect (PCE)

MRSA cells, initially at a concentration of approximately 2×10^6 CFU mL^{-1}, were cultured in tryptic soy broth (TSB) medium supplemented with compound **5p** at concentrations of 2× MIC and 3× MIC for a duration of 4 hours at 37 °C. Dimethyl sulfoxide (DMSO) at a final concentration of 0.32% (v/v) served as a control treatment. After treatment, the cultures were subjected to centrifugation and washing three times in sterile saline at 3000 revolutions per minute (rpm) for 15 minutes to remove the compound. The washed cells were then transferred to fresh TSB and incubated at 37 °C. The viable bacterial count, expressed as CFU mL^{-1}, was determined from serial dilutions of aliquots in sterile saline, which were immediately plated onto TSB agar at various time points post-incubation: 2, 3, 4, 5, 6, 7, 8, 11, 14, and 17 hours. PCE was calculated using a specified formula:

$$\mathrm{PCE} = t - c,$$

where t is the time needed for a log increase in counts in experimental groups and c is the time needed for a log increase in counts in control groups. All the experiments were repeated 2 times.

Plasma protein binding

The *in vitro* plasma protein binding characteristics of **5p** were examined using Thermo Scientific™ rapid equilibrium dialysis polypropylene 96-well plates. The experimental setup consisted of two adjacent chambers per insert, separated by an 8000 MWCO dialysis membrane. One chamber was filled with 1100 μL of plasma, while the other contained 350 μL of dialysate buffer (PBS buffer at pH 7.4). The dog plasma utilized for this investigation was sourced from Jiulong Biology in Zhengzhou, China. To prepare for the assay, a 10 mM stock solution of **5p** was created and subsequently diluted 1 : 50 with water. Using an automated liquid handling robot, 200 μL of this diluted solution, along with a control compound (sarolaner, demonstrating protein binding exceeding 99%), were added to the wells containing plasma. The plates were sealed and incubated on a shaker at 37 °C for 4 hours. Each experiment was conducted in quadruplicate using dog plasma. Following the assay, plasma protein binding was evaluated by precipitating the proteins with acetonitrile (ACN) in both plasma and PBS samples. Drug concentrations were quantified *via* LC-MS/MS, as detailed in the literature.[22] The percentage of bound compounds was determined from peak areas using eqn (1) and (2):

$$\%\ \text{free} = (\text{concentration buffer chamber}/\text{concentration plasma chamber}) \times 100\% \quad (1)$$

$$\%\ \text{bound} = 100\% - \%\ \text{free} \quad (2)$$

Confocal laser scanning microscopy

During the logarithmic phase of growth, both MRSA and *E. coli* cultures were subjected to centrifugation at 5000 rpm for 10 minutes. The resulting cell pellets were then washed twice with phosphate-buffered saline (PBS, 10 mM, pH 7.2) to remove any residual media components. Subsequently, the cells were resuspended in PBS to a concentration of 2×10^6 CFU mL^{-1}, corresponding to an optical density at 600 nm (OD_{600}) of 0.2–0.4. The bacterial suspensions were then treated with compound **5p** at a concentration equivalent to three times the minimum inhibitory concentration (3× MIC) and incubated at 37 °C for 8 hours. Following incubation, the nucleic acid stains SYTO 9 and propidium iodide (PI) were introduced to the cell suspensions, which were further incubated for 30 minutes in the dark to allow for dye penetration and binding. The stained cells were then examined under a confocal laser scanning microscope to assess membrane integrity. A control group was established

by treating the cells with an equal volume of PBS instead of **5p**. All experiments were performed in duplicate to ensure reproducibility.

Intracellular K^+ ion leakage assay

Potassium ion (K^+) efflux from MRSA and *E. coli* cells was quantified using an atomic absorption spectrophotometer (AA320N, China). The procedure for measuring K^+ release was based on a previously published method.[23] Specifically, cultures of MRSA and *E. coli* in the mid-logarithmic phase, after 6 hours of growth, were harvested by centrifugation at 10 000 rpm for 5 minutes. The cell pellets were then washed and resuspended in a mixture of 10 mM HEPES buffer (pH 7.3) and 5 mM glucose at a 1 : 1 ratio. The bacterial concentration was standardized to approximately 2×10^6 CFU mL^{-1}. Aliquots of 1 mL of these suspensions were incubated with compound **5p** at a concentration of 3 times the minimum inhibitory concentration (3× MIC) at 37 °C for various durations. Following incubation, the supernatants were obtained by centrifugation, and the K^+ content was determined using the atomic absorption spectrophotometer. A control experiment, in which compound **5p** was replaced with an equal volume of phosphate-buffered saline (PBS), was also conducted. Each experimental condition was replicated twice to ensure the reliability of the results.

Depolarization assay of cell membrane

Cultures of MRSA and *E. coli* were grown for 6 hours to reach the mid-logarithmic phase and subsequently collected by centrifugation at 10 000 rpm for 5 minutes. The cell pellets were washed and resuspended in a solution containing 100 mM potassium chloride, 5 mM HEPES buffer (pH 7.3), and 5 mM glucose mixed in equal proportions (1 : 1 : 1). A volume of 150 μL of this bacterial suspension was then added to a tube containing the membrane potential-sensitive dye DiSC3(5) (final concentration 8 μM, volume 50 μL). The cell suspension was preincubated at 37 °C for 40 minutes for MRSA and 80 minutes for *E. coli* to allow the dye to equilibrate across the bacterial membranes. For fluorescence monitoring, the excitation and emission wavelengths were set at 622 nm and 670 nm, respectively. Following preincubation, the treated suspension was carefully transferred to a fresh tube containing 10 μL of compound **5p** at a concentration of 3× MIC. The fluorescence intensity was then measured as an indicator of membrane potential changes. A control experiment was conducted by treating the preincubated bacterial and dye mixture with water (10 μL) instead of **5p**. This control was used to assess the baseline fluorescence in the absence of the test compound.

In vivo antibacterial activity

All animal procedures were performed in accordance with the Guidelines for Care and Use of Laboratory Animals of China Three Gorges University and approved by the Animal Ethics Committee of China Three Gorges University. Male and female Kunming mice, averaging 20 g in weight, were subjected to immunosuppression *via* daily intraperitoneal injections of cyclophosphamide for three consecutive days. Methicillin-resistant *S. aureus* (MRSA) was cultured on Mueller–Hinton agar (MHA) plates and incubated at 37 °C overnight to reach a concentration of 6×10^7 CFU mL^{-1} for subsequent corneal infection. Prior to inoculation, mice were anesthetized with an intraperitoneal injection of 2.5% avertin at a dosage of 400 mg kg^{-1}. The corneal surfaces were then gently abraded with a sterile needle, followed by the application of 20 μL of the MRSA suspension. Twenty-four hours post-infection, the animals were randomly assigned into four groups, each comprising six mice: a negative control receiving 5% glucose, a positive control treated with 5% vancomycin, and two experimental groups administered

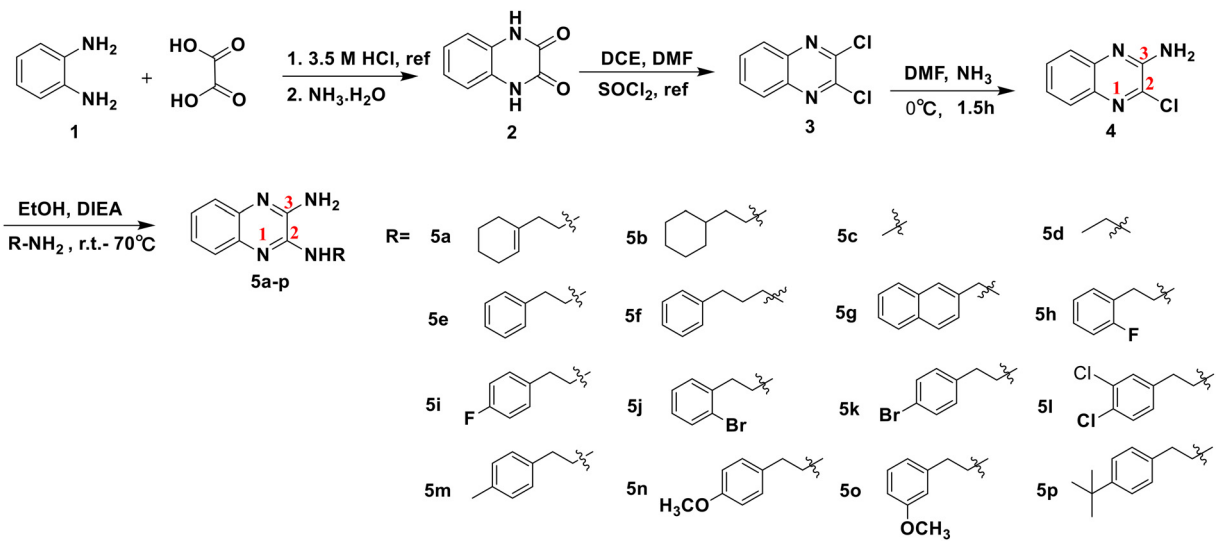

Scheme 1 Synthesis of derivatives **5a**–**5p**.

with either 3.0 mg mL^{-1} or 6.0 mg mL^{-1} of **5p** *via* topical application thrice daily for one week. Upon completion of the study, the mice were euthanized, and the infected corneas were harvested for bacterial viability assessment using the plate counting technique.

Results and discussion

Synthetic chemistry

The process of producing quinoxaline derivatives **5a–5p** is outlined in Scheme 1 using *o*-phenylenediamine as the main raw material. First, *o*-phenylenediamine reacted with glycolic acid under acidic circumstances to generate compound **2**, which subsequently underwent nucleophilic attack and elimination in the presence of DMF to yield compound **3**. A mixture of **3** and ammonia solution in DMF was stirred at 0 °C for 1.5 h to obtain the intermediate **4**. Next, **4** was reacted with a series of amino compounds to give the target derivatives **5a–5p**.

In vitro antibacterial activity

The newly synthesized compounds (**5a–5p**) were screened for their antimicrobial activity. Four drug-sensitive strains (*S. aureus* RN4220, *B. subtilis* 168, *E. coli* DH5 and *P. aeruginosa* PAO1) and three drug-resistant bacterial strains (MRSA USA300, VRE and *K. pneumoniae*) were selected to evaluate the effectiveness of the test compounds. The novel derivatives were subjected to minimum inhibitory concentration (MIC) determination by microdilution method and the results are listed in Table 1. The data showed that compounds **5m–5p** exhibited good to moderate antibacterial activity against *S. aureus* (4–16 μg mL^{-1}) and *B. subtilis* (8–32 μg mL^{-1}), while **5e–5g** displayed moderate to mild inhibitory activity against these two strains (*S. aureus*: 32 μg mL^{-1}; *B. subtilis*: 32–64 μg mL^{-1}). Compound **5p** showed the highest activity against *S. aureus* and *B. subtilis*, with MICs of 4 and 8 μg mL^{-1}, respectively.

Compounds **5a–5d**, with aliphatic alkyl substitution on the C-2 side chain, did not exhibit any antibacterial activity against all the tested strains. However, when aromatic rings were attached to the C-2 side chains, the antibacterial activity of compounds **5e–5g** was significantly increased, with MIC values of 32–64 μg mL^{-1} against Gram-positive bacteria. These results indicated that aromatic ring substituents on C-2 side chains are preferable to aliphatic alkyl groups. Thus, in order to further understand the influence of different substituents of the aromatic ring on antibacterial activity, derivatives **5h–5p** were designed and synthesized in the subsequent modification. Compounds **5h–5l**, with an electron-withdrawing group attached on the aromatic ring, showed mild and weak activity (64–128 μg mL^{-1}) regardless of whether the substituents were in the *ortho* or *para* site. In particular, compound **5l**, with two electron-absorbing substituents on its benzene ring, exhibited no antibacterial activity with MIC values of >128 μg mL^{-1}. Nevertheless, compounds **5m–5p** displayed good antibacterial activity against Gram-positive bacteria (4–16 μg mL^{-1} against *S. aureus*; 8–32 μg mL^{-1} against *B. subtilis*) when there was an electron-donating group attached to the aromatic ring. By comparing the structure and antibacterial activity of compounds **5m–5p**, it is possible to deduce that the activity of the compounds increased with the enhancement of the electron-donating ability of the substituents on the aromatic ring. Compound **5p**, with a *tert*-butyl group attached, exhibited the most electron-donating capacity and displayed the highest activity. Furthermore, compounds **5m–5p** showed obvious advantages in expanding the antibacterial spectrum, exhibiting remarkable efficacy against Gram-positive bacteria and conspicuous inhibition against Gram-negative strains. Compounds **5m** and **5n** displayed moderate inhibitory effects

Table 1 *In vitro* antibacterial activity of the synthesized derivatives (MIC: μg mL^{-1})

	Drug-sensitive bacteria				Drug-resistant bacteria		
Strain	*S. aureus*	*B. subtilis*	*E. coli*	*P. aeruginosa*	MRSA	*K. pneumonia*	VRE
5a	64	128	>128	>128	>128	>128	>128
5b	128	>128	>128	128	128	>128	>128
5c	128	64	128	128	>128	>128	>128
5d	128	128	>128	128	>128	>128	128
5e	32	64	128	128	>128	>128	>128
5f	32	64	128	>128	128	128	128
5g	32	32	64	>128	64	>128	>128
5h	64	128	128	128	128	>128	128
5i	64	64	128	>128	>128	128	128
5j	128	64	>128	128	128	64	128
5k	64	64	128	128	>128	>128	>128
5l	>128	>128	>128	>128	>128	>128	>128
5m	16	32	32	64	32	64	>128
5n	16	16	32	128	16	64	>128
5o	8	32	16	64	16	64	128
5p	4	8	4	64	8	128	>128
KAN[a]	1	0.5	1	4	1	4	8

[a] KAN: kanamycin.

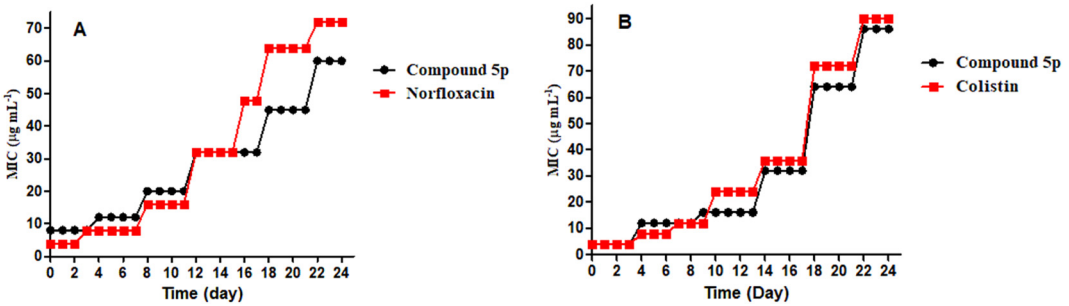

Fig. 3 Propensity to induce bacterial resistance of **5p** against (A) MRSA, (B) *E. coli*.

with MICs of 32 μg mL^{-1} against *E. coli*, while **5o** and **5p** showed good antibacterial activity (4–16 μg mL^{-1}) against this pathogen.

The broad-spectrum antibacterial agents **5m–5p** were then further evaluated against a variety of drug-resistant bacteria, such as MRSA, β-lactam-resistant *K. pneumoniae*, and VRE (Table 1). The data showed that compounds **5m–5p** displayed good to moderate antibacterial activity against MRSA with MIC values of 8–32 μg mL^{-1} and mild activity against *K. pneumoniae* with MICs of 64–128 μg mL^{-1}. Among them, compound **5p** was the most active one with MIC of 8 μg mL^{-1} against MRSA. The effectiveness of these compounds against Gram-positive, Gram-negative and drug-resistant bacteria indicates their potential as antibacterial leads and warrants further investigation.

Propensity to develop bacterial resistance

Antimicrobial resistance is a severe problem in anti-infective therapy and is of great concern. Many therapeutic agents, including erythromycin, tetracycline and sulfonamides, have been pulled from the market or moved to the second line of treatment owing to bacterial resistance. Hence, it is vital to monitor the development of bacterial resistance to this type of compounds. The current study assessed the development of resistance of MRSA and *E. coli* to **5p** using norfloxacin and colistin as the positive controls. The data in Fig. 3A show that the rate of increase in MIC values was slightly higher than that of the control group during the first 15 days of the experiment. However, the results reversed in the last 9 days, and the MIC values were considerably higher in the norfloxacin group than that in the administration group. For *E. coli* in Fig. 3B, both compound **5p** and colistin showed a similar increase in MIC values, suggesting that the two groups displayed the same results in terms of drug resistance.

Bactericidal time-kill kinetics

To study the bactericidal impact of compound **5p** on both Gram-positive and Gram-negative bacteria, bactericidal tests against MRSA and *E. coli* were performed using norfloxacin and colistin as the positive controls. The data in Fig. 4 show that compound **5p** demonstrated clear bactericidal action against MRSA at 3× MIC (>6 $\log_{10}$ CFU mL^{-1} reduction), but limited bacteriostatic activity at 2× MIC. In contrast, norfloxacin showed only inhibitory rather than bactericidal effects at 2× MIC concentrations. However, compound **5p** was significantly inferior to MRSA in terms of bactericidal activity against *E. coli*, displaying only inhibitory effects even at 3× MIC, whereas the positive group (colistin) showed remarkable bactericidal activity at 2× MIC.

Cytotoxicity evaluation of compounds

Many commonly used antimicrobial agents, such as sparfloxacin, gatifloxacin, kanamycins and chloramphenicol, have gradually entered the second line or even been withdrawn from the market due to their toxicity. For this reason, cytotoxicity assessment is crucial in the process of structural modification. Compounds **5e–5g** and **5m–5p** were

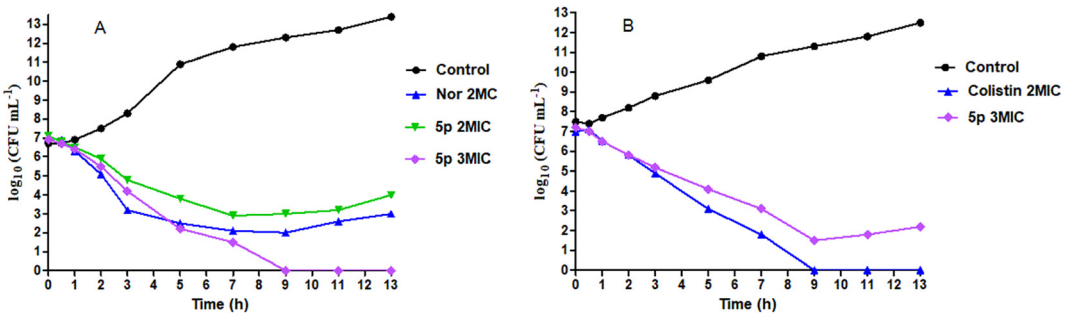

Fig. 4 Time-kill kinetics of **5p** against (A) MRSA, (B) *E. coli*.

Table 2 Cytotoxicity evaluation of **5e–5g** and **5m–5p** against MCF-7, HEK-293 and HK-2 cells

Compound	IC_{50}[a,b] (μg mL^{-1})		
	MCF-7 (breast cancer)	HEK-293 (human epithelial kidney cells)	HK-2 (proximal tubule epithelial cells)
5e	72.34 ± 4.21	123.46 ± 5.79	130.26 ± 5.85
5f	68.67 ± 4.56	125.61 ± 6.34	140.77 ± 6.21
5g	69.72 ± 5.13	130.79 ± 7.23	146.53 ± 5.56
5m	70.90 ± 4.83	135.66 ± 6.01	149.62 ± 6.80
5n	71.55 ± 5.56	128.63 ± 5.98	138.52 ± 6.99
5o	74.68 ± 3.98	130.31 ± 7.08	142.04 ± 7.22
5p	72.55 ± 5.06	129.09 ± 6.14	145.60 ± 5.06
5-Fu[c]	0.85 ± 0.20	—	—

[a] IC_{50} is the concentration required to inhibit 50% of cell growth. [b] Results are expressed as the mean ± S.D. of three independent experiments; the incubation time for the cells and samples was 24 hours. [c] 5-FU: 5-fluorouracil.

then selected for evaluating the cytotoxicity against one human cancer cell line (MCF-7) and two human normal cell lines (HEK-293 and HK-2) using the MTT assay. As can be seen from the data in Table 2, the compounds tested exhibited low toxicity to both normal cells, with IC_{50} values of 120–155 μg mL^{-1}, while their IC_{50} values were about 70 μg mL^{-1} for MCF-7 cells. These results clearly show that these compounds have no influence on the viability of mammalian cells at their antibacterial MICs.

Biofilm disruption assay

The evolution of drug resistance in bacteria is closely linked to the production of bacterial biofilm. Once biofilm forms, the therapeutic benefits will be significantly diminished.[24] As a result, we further evaluated the efficiency of **5p** to eradicate the established biofilms of MRSA and *E. coli*. After incubation of 48 h, the mature MRSA and *E. coli* biofilms were established and then treated with different concentrations of **5p**. The data in Fig. 5 show that the number of viable bacteria (MRSA cells) in biofilms decreased from 13.5 $\log_{10}$ CFU mL^{-1} to 11.8, 7.3 and 0 $\log_{10}$ CFU mL^{-1} at 8 (MIC), 16 (2× MIC) and 24 μg mL^{-1} (3× MIC). It should be noted that at high concentrations of **5p**, the number of viable bacteria directly reduced to 0, suggesting that the established biofilms disappeared completely. For *E. coli*, the cell viability in biofilms was decreased from 18.5 $\log_{10}$ CFU mL^{-1} to 16.8, 14.5 and 7.4 $\log_{10}$ CFU mL^{-1}, corresponding to 4 (1× MIC), 8 (2× MIC) and 16 μg mL^{-1} (4× MIC), respectively. These results once again demonstrated the excellent antibacterial properties of compound **5p**.

Postcontact effect (PCE) of 5p

In order to further confirm the antibacterial activity of this class of compounds, we carried out a research on the postcontact effect (PCE) of **5p** against MRSA. The PCE is based on the post-antibiotic effect and evaluates microbial growth inhibition following antibiotic removal. The data in Fig. 6 show that the viable counts of MRSA decreased significantly (>3 $\log_{10}$ CFU mL^{-1} reduction) after **5p** treatment. The antibiotics were then removed. The duration of inhibition was dose-dependent. The number of bacteria increased significantly after 3 hours at 2× MIC, while the duration was up to 5 hours at 3× MIC. Furthermore, the CFU mL^{-1} value of pretreated cultures at less than 24 hours were lower than that of the untreated cultures. The PCE results showed that the growth rate of viable bacteria was greatly impacted and did not recover in less than 24 hours, even after antibacterial drugs were removed.

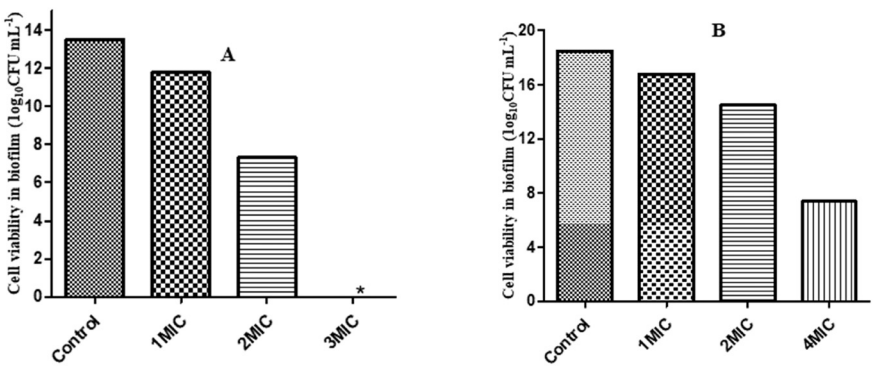

Fig. 5 Biofilm dispersion by **5p**: (A) cell viability in biofilms of MRSA and (B) *E. coli*, obtained by plating and counting the viable bacteria after treating.

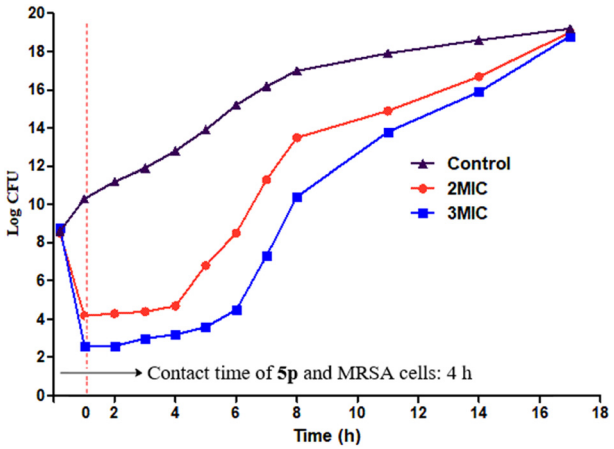

Fig. 6 Postcontact effects (PCEs) of **5p** at 2× MIC and 3× MIC.

Structure–activity relationship (SAR) analysis

Preliminary SARs of quinoxaline derivatives might be drawn from the current study (Fig. 7). It is possible to deduce that aromatic ring substituents on C-2 side chains are preferable to aliphatic alkyl groups by comparing the antibacterial activity between compounds **5a–5d** and **5e–5g**. The influence of different substituents on the aromatic ring of C-2 is of great importance. Compounds **5h–5l**, with an electron-withdrawing group attached on the aromatic ring, showed mild and weak activity (64–128 μg mL^{-1}) regardless of whether the substituents were in the *ortho* or *para* site. In particular, compound **5l**, with two electron-absorbing substituents on its benzene ring, exhibited no antibacterial activity with a MIC value of >128 μg mL^{-1}. These results indicate that the existence of electron-absorbing substituents is disadvantageous to antibacterial activity against Gram-positive bacteria. Nevertheless, compounds **5m–5p** displayed good antibacterial activity against Gram-positive bacteria when there was an electron-donating group attached to the aromatic ring. By comparing the structure and antibacterial activity of compounds **5m–5p**, it is possible to deduce that the activity of the compounds increased with the enhancement of the electron-donating ability of the substituents on the aromatic ring. Compound **5p**, with a *tert*-butyl group attached, exhibited the most electron-donating capacity and displayed the highest activity. Furthermore, **5m–5p** showed a broad antibacterial spectrum, exhibiting remarkable efficacy against Gram-positive bacteria and conspicuous inhibition against Gram-negative strains. These results suggest that the introduction of electron-donating groups in the aromatic ring can not only improve the antibacterial activity, but also enlarge the antibacterial spectrum and enhance the effects against Gram-negative bacteria.

Drug-like properties and ADME process

The drug-likeness evaluation of some active compounds was also performed with the aid of web-based Molsoft (**https://www.molsoft.com/molprop/**) and Molinspiration Cheminformatics (**https://www.molinspiration.com/**) based on Lipinski's rule of five. This program provides the information regarding the possibility of these derivatives as clinical drugs. If a compound displays the potential to become a commercial drug, its molecular weight (MW) is likely to be less than or equal to 500, clog *P* is less than or equal to 5, the number of HBA is less than or equal to 10, the number of HBD and RB is less than or equal to 5.[25] The absorption, distribution, metabolism and excretion (ADME) properties provide an insight into the pharmacokinetic process of the tested compounds (**5m–5p**). The oral bioavailability (OB) was analyzed by ACD/I-Lab 2.0 (**https://ilab.acdlabs.com/iLab2/index.php**). The human intestinal absorption (HIA) rate, Madin–Darby canine kidney (MDCK) cell permeability, blood–brain barrier (BBB) penetration, and plasma protein binding (PPB) rate were calculated through a web-based pre-ADME program (**https://preadmet.bmdrc.kr/**). The data (Table 3) show that all of the drug-like characteristics such as MW, clog *P*, HBA, HBD, and RB were within the acceptable range, consistent with Lipinski's rule of

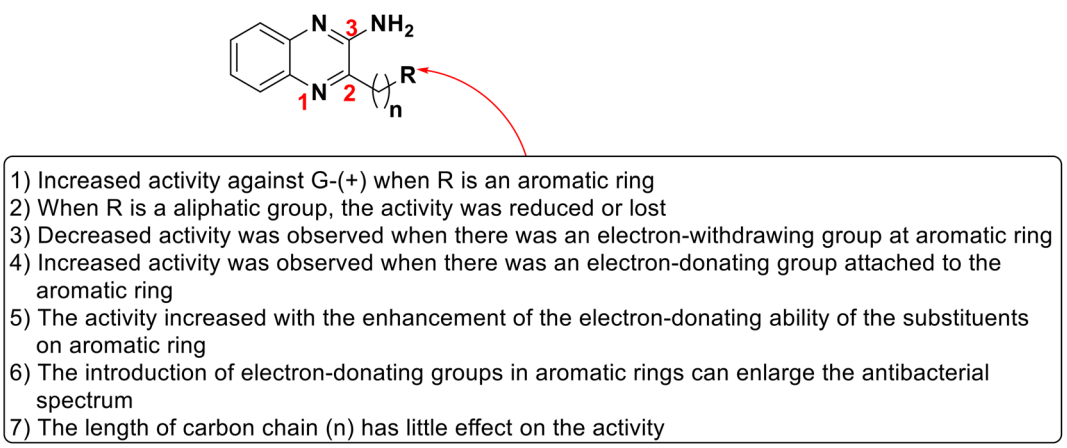

Fig. 7 Structure–activity relationships of quinoxaline derivatives.

Table 3 Drug-like properties and ADME process

Compds	MW	OB	HIA (%)	PPB (%)	BBB (C_{brain}/C_{blood})	MDCK (nm s^{-1})	Lipinski's rule
5m	278.35	Moderate	63.06	76.20	0.10	20.36	Suitable
5n	294.36	Moderate	71.25	68.12	0.12	18.45	Suitable
5o	294.36	Moderate	70.46	72.55	0.12	19.61	Suitable
5p	320.43	Good	85.07	85.49	0.15	21.56	Suitable

MW: molecular weight. OB: oral bioavailability; poor: OB ≤30%; moderate: 30% ≤ OB ≤ 70%; good: OB ≥70%. HIA: human intestinal absorption; poorly absorbed: 0–20%; moderately absorbed: 20–70%; well absorbed: 70–100%. PPB: plasma protein binding; strongly bound: ≥90%; moderately bound: 60–90%; weakly bound: ≤60%. BBB: blood–brain barrier penetration (C_{brain}/C_{blood}); high absorption to CNS: ≥2.0; moderate absorption to CNS: 0.1–2.0; low absorption to CNS: <0.1. MDCK: Madin–Darby canine kidney cell permeability; low permeability: ≤25; moderate permeability: 25–500; high permeability: >500.

Table 4 Protein binding of **5p** and control group after 4 h of incubation in plasma

Entry	% average recovery	SD[a]	% unbound	% bound	SD
5p	73.5	15.6	7.32	92.6	0.002
Control[b]	71.2	12.3	0.45	99.5	0.001

[a] Results are expressed as the mean ± S.D. of four independent experiments (n = 4). [b] Control: sarolaner, >99% protein bound.

five. In general, the OB levels of the compounds correlated with their HIA rates. Compounds **5m**–**5p** displayed good to moderate oral bioavailability and moderate plasma protein binding rate (68.12–85.07%). Among them, **5p** exhibited the best bioavailability and the highest human intestinal absorption rate, with HIA values of 85.07%. BBB and PPB are important parameters to assess the distribution of compounds in the human body. BBB penetration represents the ability of compounds to pass the BBB, which is a prerequisite of the peripheral compounds to produce CNS effects as well. All the tested compounds demonstrated moderate blood–brain barrier penetration and plasma protein binding rate. MDCK cells can be used for the prediction of drug renal excretion ability. The data showed that **5m**–**5p** displayed low permeability to the kidney cells, suggesting that the time required to excrete these compounds is high. This result indicated that this type of compounds exhibited an extended duration of action within the body.

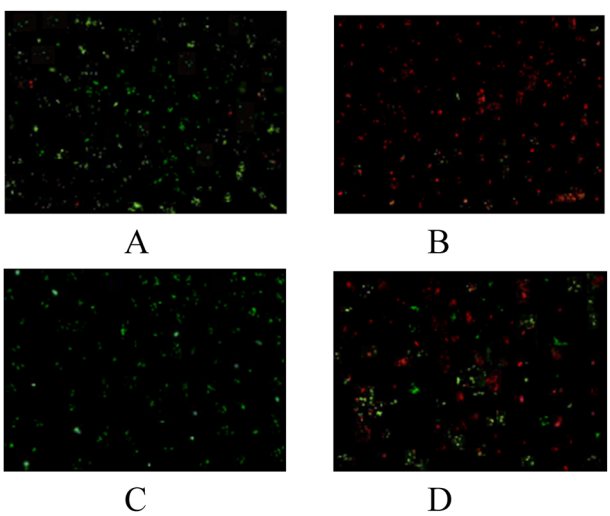

Fig. 8 Fluorescence microscopy of **5p** induced permeabilization of MRSA and *E. coli* by SYTO 9 and PI staining. MRSA cells were treated with PBS (A, control group) and **5p** (B, 3× MIC); *E. coli* cells were treated with PBS (C, control group) and **5p** (D, 3× MIC).

Plasma protein binding

The protein binding affinity of compound **5p** was evaluated *in vitro* with sarolaner, a compound known for its >99% plasma protein binding, serving as a control. The study aimed to understand the interaction between the candidate drugs and plasma proteins, which is crucial for their pharmacokinetics, including efficacy, safety, and distribution. Rapid equilibrium dialysis was conducted using dog plasma as the medium.[22] The results demonstrated that **5p** has a high affinity for plasma proteins, with over 92% of it bound to these proteins. LC-MS/MS analysis showed that the free fraction of **5p** in dog plasma was 7.32%. Both **5p** and the control compound exhibited recoveries above 70%, as detailed in Table 4.

Effect on membrane permeabilization

Confocal laser scanning microscopy. In both the control and the **5p**-treated groups, the presence of viable and non-viable bacteria was discerned through fluorescence staining with SYTO 9 and propidium iodide (PI), followed by examination under confocal laser scanning microscopy (CLSM). SYTO 9, a fluorescent dye capable of permeating all cell membranes, was utilized to label nucleic acids, resulting in green fluorescence indicative of viable cells. Conversely, propidium iodide (PI), which is membrane-impermeant, exclusively stains the nucleic acids of bacteria with compromised cell membranes, exhibiting red fluorescence.

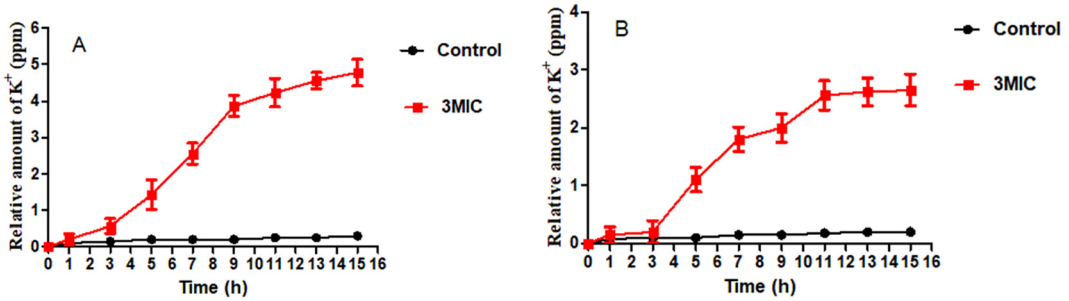

Fig. 9 Effects of **5p** on the amount of K^+ released from (A) MRSA and (B) *E. coli*.

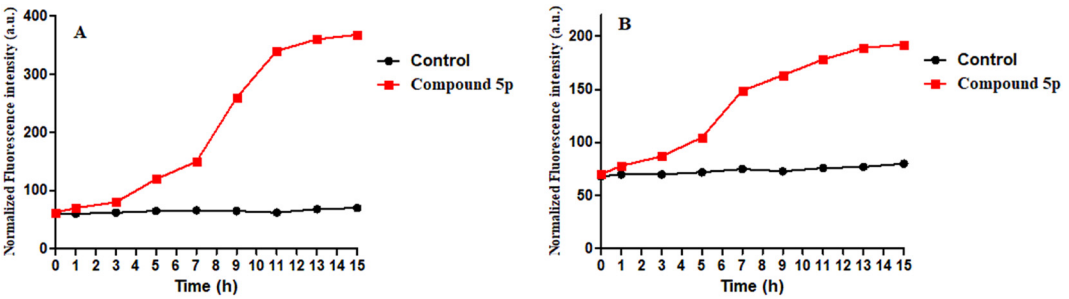

Fig. 10 Membrane depolarization against (A) MRSA (3× MIC) and (B) *E. coli* (3× MIC).

Consequently, the presence of green fluorescence in bacterial cells was interpreted as a sign of intact cell membranes and cellular viability, whereas red fluorescence indicated compromised membranes and cell death. The experimental findings demonstrated a comparable trend in the fluorescence intensity between MRSA and *E. coli* upon staining with SYTO 9/PI. Fig. 8 illustrates a pronounced predominance of viable cells over non-viable ones in the control group. After **5p** treatment, a significant augmentation in the count of non-viable cells for both MRSA and *E. coli* was observed. The observed escalation in red fluorescence is indicative of the bactericidal effect of **5p**, which inflicted lethal damage upon the bacterial membranes.

Intracellular K^+ ion leakage assay. To investigate the impact of **5p** on cellular membranes, the study further focused on the permeability changes of bacterial membranes to potassium ions. The efflux of K^+ from MRSA and *E. coli* cells was quantified using an atomic absorption spectrophotometer. The experimental procedure for measuring K^+ release adhered to the protocols previously established in the scientific literature.[23] Fig. 9 presents the concentration of potassium ion efflux from MRSA and *E. coli* following incubation with **5p** (3× MIC) for different times. The data show that a significant increase in K^+ efflux was observed in the experimental groups, indicative of altered membrane permeability. In contrast, the control groups exhibited negligible changes in K^+ efflux, suggesting that the observed effects were specifically attributable to the **5p** treatment. Upon comparative analysis of the K^+ release profiles for both bacterial strains, it was observed that compound **5p** exerted a more pronounced impact on the cell membrane integrity of Gram-positive bacteria MRSA, as opposed to the Gram-negative bacteria *E. coli*.

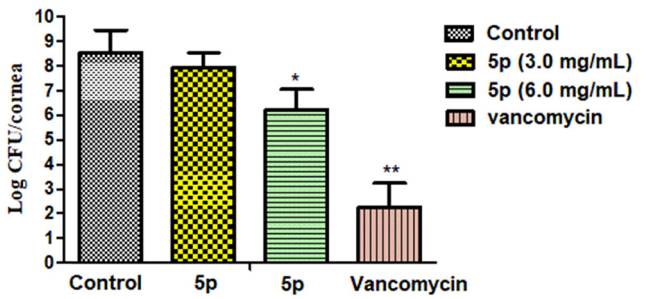

Fig. 11 *In vivo* antibacterial activity of **5p** (3.0 mg mL^{-1} and 6.0 mg mL^{-1}) against MRSA (n = 6).

Depolarization assay of cell membrane. To determine if the molecules function by depolarizing the bacterial cell membrane, we utilized $DiSC_3(5)$, a fluorescent probe sensitive to membrane potential. Typically, this dye could be absorbed by the bacterial membrane due to the potential gradient, which resulted in a reduction of its fluorescence intensity as a consequence of self-quenching. Upon the loss of membrane potential, the dye is released into the surrounding solution, thereby increasing the fluorescence intensity. Significantly, the application of **5p** to bacterial strains resulted in an increased fluorescence intensity of DiSC3(5) in both MRSA and *E. coli* (Fig. 10). Moreover, the experimental data revealed a pronounced difference in fluorescence intensity between MRSA and *E. coli*, with MRSA exhibiting a significantly higher fluorescence intensity. These observations strongly suggested

that **5p** was capable of depolarizing the membrane potential in both Gram-positive and Gram-negative bacteria.

In vivo antibacterial activity

Preliminary *in vivo* antibacterial tests of **5p** were also carried out using a mouse corneal infection model against MRSA. The drug was given by local smear. The corneal infection model was induced by carefully abrading the cornea to create a controlled injury, which was then followed by topical application of an incubated bacterial suspension to the compromised ocular surface. After infection, compound **5p** was administered topically at concentrations of 3.0 and 6.0 mg mL^{-1}, with applications occurring three times daily for a period of one week. 5% glucose and 5% vancomycin solution were used as negative control and positive control, respectively. The experimental findings (Fig. 11) indicated that in comparison to the negative control group, compound **5p** at 6.0 mg mL^{-1} and vancomycin significantly reduced the viable bacterial count in the infected corneas by 2.34 and 6.30 log units, respectively. Nevertheless, compound **5p** at 3.0 mg mL^{-1} did not exhibit a statistically significant difference in reducing the viable bacterial count when compared to the negative control group. The experimental data indicated that compound **5p** exhibited the potential to be an efficacious antibacterial agent *in vivo* only at higher concentrations, thereby warranting further exploration and investigation.

Conclusion

In the current study, we have designed and prepared a diverse array of quinoxaline-based compounds, which were derived from *o*-phenylenediamine. Among them, compounds **5m–5p** displayed good to moderate antibacterial activity with MICs of 4–16 μg mL^{-1} against *S. aureus*, 8–32 μg mL^{-1} against *B. subtilis*, 8–32 μg mL^{-1} against MRSA and 4–32 μg mL^{-1} against *E. coli*, respectively. Compound **5p**, identified as a potent broad-spectrum antibacterial agent, demonstrated the strongest inhibitory effects against a range of bacterial strains and low cytotoxicity, thereby warranting further investigation. Compound **5p** not only demonstrated the ability to disperse established bacterial biofilms but also induced a slower development of bacterial resistance compared to norfloxacin. Moreover, bactericidal time-kill kinetic studies revealed that at a high concentration of 3× MIC, compound **5p** was capable of directly killing MRSA cells. The subsequent PCE results showed that the growth rate of viable bacteria (MRSA) was greatly impacted and did not recover in less than 24 hours, even after antibacterial agent **5p** was removed. The drug-like properties and ADME prediction exhibited that **5m–5p** obeyed Lipinski's rule of five and maintained moderate to good oral bioavailability and human intestinal absorption rate. Mechanistic investigations have elucidated that compound **5p** exerted its antibacterial effect by compromising the structural integrity of bacterial cell membranes, resulting in the leakage of intracellular constituents and ultimately causing bacterial demise. Further studies *in vivo* have demonstrated that **5p** exhibited potent antibacterial efficacy against MRSA in murine corneal infection models, particularly at elevated concentrations. The current dataset has also been meticulously analyzed to delineate the structure–activity relationships (SARs) of the synthesized compounds.

Data availability

The authors confirm that the data supporting the findings of this study are available within the article and/or its ESI.†

Conflicts of interest

The authors confirm that this article content has no conflict of interest.

Acknowledgements

This work was supported by the open fund of the State Key Laboratory of New Anti-Infective Drugs (grant number SKL2024003).

References

1 C. H. Wang, Y. H. Hsieh, Z. M. Powers and C. Y. Kao, *Int. J. Mol. Sci.*, 2020, **21**(3), 1061.
2 M. K. Byrne, S. Miellet, A. McGlinn, J. Fish, S. Meedya, N. Reynolds and A. M. Oijen, *BMC Public Health*, 2019, **19**(1), 1425.
3 L. F. E. Moor, T. R. A. Vasconcelos, R. D. R. Reis, L. S. Pinto and T. M. Costa, *Mini-Rev. Med. Chem.*, 2021, **21**(16), 2209.
4 I. A. Graciano, A. S. Carvalho and V. F. Ferreira, *Med. Chem.*, 2022, **18**(5), 521.
5 M. Owais, A. Kumar, S. M. Hasan, K. Singh, I. Azad, A. Hussain and M. Akil, *Mini-Rev. Med. Chem.*, 2024, **24**(13), 1238.
6 S. Rajendran, K. Sivalingam, R. P. K. Jayarampillai, W. L. Wang and C. O. Salas, *Chem. Biol. Drug Des.*, 2022, **100**(6), 1042.
7 S. Verma, S. Lal, R. Narang and K. Sudhakar, *ChemMedChem*, 2023, **18**(5), 571.
8 L. F. E. Moor, T. R. A. Vasconcelos, R. R. R. Da, L. S. S. Pinto and T. M. Da Costa, *Mini-Rev. Med. Chem.*, 2021, **21**(16), 2209.
9 S. Verma, S. Lal, R. Narang and K. Sudhakar, *ChemMedChem*, 2023, **18**(5), 571.
10 T. Odagiri, H. Inagaki, Y. C. Sugimoto, M. Nagamochi, R. N. Miyauchi, J. Kuroyanagi, T. Kitamura, S. Komoriya and H. Takahashi, *J. Med. Chem.*, 2013, **56**, 1974.
11 H. A. Alzahrani, *Braz. J. Microbiol.*, 2023, **54**(4), 2799.
12 E. Sadowski, B. Bercot, A. Chauffour, C. Gomez, E. Varon, M. Mainardis, W. Sougakoff, C. Mayer, E. Sachon, G. Anquetin and A. Aubry, *Bioorg. Med. Chem. Lett.*, 2022, **1**, 55.
13 J. Hoque, M. M. Konai, S. S. Sequeira and S. Samaddar, *J. Med. Chem.*, 2016, **59**, 10750.

14 B. Ding, Q. Guan, J. P. Walsh, J. S. Boswell, T. W. Winter, E. S. Winter, S. S. Boyd, C. Li and P. B. Savage, *J. Med. Chem.*, 2002, **45**, 663.
15 A. Scaiola, M. Leibundgut, D. Boehringer, P. Caspers, D. Bur, H. H. Locher, G. Rueedi and D. Ritz, *Sci. Rep.*, 2019, **9**(1), 5634.
16 Z. H. Jian, L. Zeng, T. J. Xu, S. Sun, S. X. Yan, L. Yang, Y. Huang, J. J. Jia and T. F. Dou, *J. Basic Microbiol.*, 2021, **61**(12), 1049.
17 X. Li, S. T. Ma, M. Yan, Y. Z. Wang and S. T. Ma, *Eur. J. Med. Chem.*, 2013, **59**, 209.
18 M. A. M. Subbaiah and N. A. Meanwell, *J. Med. Chem.*, 2021, **64**(19), 14046.
19 K. Bundit, P. Bongkochawan, T. Paptawan, L. Naruedon, K. Pharit, P. Auradee, K. Sombat, S. Patchreenart, H. Supa, S. Jidapa, S. Khomson, S. Sanya and P. Pornpan, *J. Chem. Inf. Model.*, 2023, **63**(9), 2707.
20 Z. W. Zhou, C. Ma, H. Y. Zhang, Y. Bi, X. Chen, Q. G. Meng and J. Y. Xu, *Eur. J. Med. Chem.*, 2013, **68**, 444.
21 J. Hoque, M. M. Konai, S. Gonuguntla, G. B. Manjunath and V. Yarlagadda, *J. Med. Chem.*, 2015, **58**, 5486.
22 G. Ines, D. H. Bernard, V. Jaspreet, L. W. Jeffrey, K. Jason, E. H. Johannes, M. N. Hanne, D. Peter and R. H. Paul, *Molecules*, 2018, **23**, 630.
23 G. Hao, Y. H. Shi, Y. L. Tang and G. W. Le, *Peptides*, 2009, **30**, 1421.
24 U. Römling and C. Balsalobre, *J. Intern. Med.*, 2012, **272**, 541.
25 E. Haar, J. T. Coll, D. A. Austen, H. M. Hsiao, L. Swenson and J. Jain, *Nat. Struct. Biol.*, 2001, **8**, 593.

